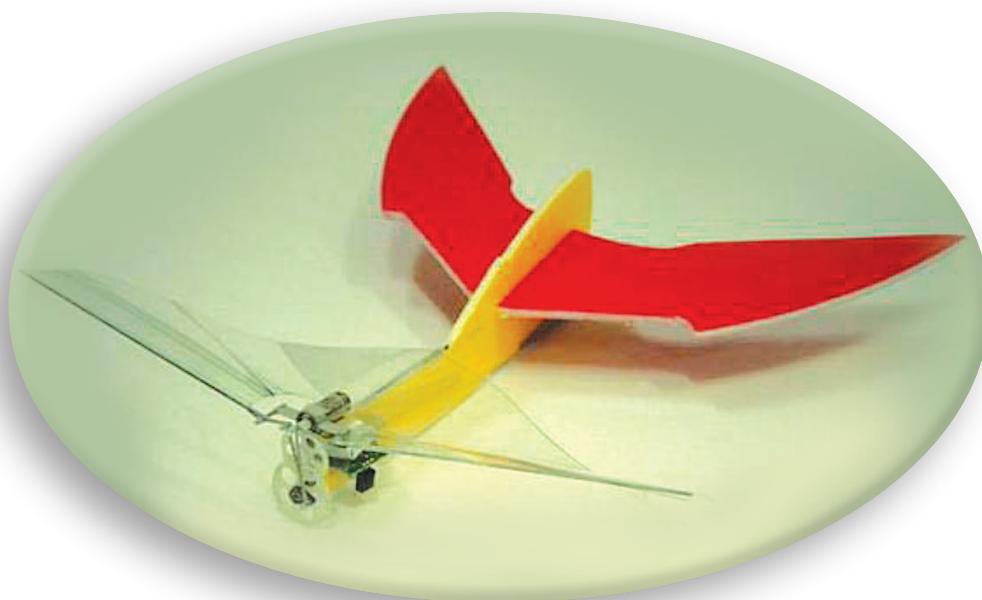# Autopilots for Ultra Lightweight Robotic Birds

AUTOMATIC ALTITUDE CONTROL AND SYSTEM INTEGRATION OF A SUB-10 G WEIGHT FLAPPING-WING MICRO AIR VEHICLE

FU-YUEN HSIAO, LUNG-JIEH YANG, SEN-HUANG LIN,
CHENG-LIN CHEN, and JENG-FU SHEN

This article discusses the altitude control of a flapping-wing micro aerial vehicle (MAV). Although the power requirement can be high for suboptimal designs, flapping flight can be an efficient way to transport a mass over a distance [1]. For example, an optimized flapping flight can require 27% less aerodynamic power than its optimal steady-flight counterpart at the scale smaller than a bird [2]. This potential for increasing efficiency as well as increased maneuverability has motivated a renewed interest in flapping flight among researchers. However, it is difficult to understand the autonomous flight of

bird-like micro robots due to limited sensing payload capacity. This article describes the first step in tackling this problem, which is the automatic altitude control of such a vehicle.

Of the flapping MAVs available, the Golden Snitch [3], named after the device referenced in the popular Harry Potter series, is the platform used for this investigation (see Figure 1). This device has a 20 cm wingspan and a gross takeoff weight (GTOW) of 8 g, which includes its fuselage, flapping wings, tail wings, a battery, a motor, and a set of gear systems. The flapping wings are driven by a motor with a four-bar linkage system. By adjusting the lengths of the four bars, various stroke angles can be employed. The stroke angle of the Golden Snitch is designed around 53° [3].

Theoretical investigations of the aerodynamics of flapping flight span over a century (e.g., [4]–[7] and citations therein). Variations of the positional angle of fore and hind wings during flight of locusts (*Schistocerca gregaria*) have been determined [7]. Experimental studies [5], [6], [8], [9] have enabled a better understanding of the natural wing articulation by insects in hover and forward flight. External or onboard cameras have been used for navigation and guidance for the flight altitude of the Delfly II MAV [10]. Unlike the experiments in this article that employ stereo vision, only one external camera was used in [10] to determine the scaled *y*-coordinate in the Delfly II experiments. A proportional control (P-control) was designed to stabilize the flight with a scaled *y*-coordinate as the feedback quantity. As a result, the throttle required trimming in advance. Modeling, dynamics, and control laws for flapping flight have been investigated [11]–[20]. Optical methods for navigation and guidance have been developed [21]–[23]. The robotic birds in [10] and [21] are twice the weight of the Golden Snitch, affording them a greater sensing payload capacity than would be possible for the Golden Snitch. Consequently, the aim of this article is not to develop a new or more sophisticated control law. Rather, this article considers the practical problems of the control law implementation and system integration using existing control technology.

The article begins by providing some background on the design and development of the mechanisms that enable the Golden Snitch to fly. Then the equations of vertical motion for this particular robotic bird are derived. Aerody-

namical and dynamical coefficients are obtained from experimental data. To keep the overall weight of the vehicle as low as possible, a commercial infrared (IR) transmission module that weighs fewer than 1 g was selected, which unfortunately constrains the communication capability. A nonintrusive method to replace a traditional onboard computer and sensors is also discussed. By using stereovision, the three-dimensional position of the Golden Snitch can be obtained [23]. Further details about the stereovision system are provided in "How Does a Stereovision System Work?". All navigational information and control commands are computed on the ground station and transmitted to the air vehicle. The control commands generated using a modified proportional feedback is shown be sufficient for achieving height control. The validity of the approach is demonstrated in numerical simulations and flight tests.

DEVELOPMENT OF THE GOLDEN SNITCH

Development History

For a flapping-wing MAV, weight is a critical issue because the low cruise speed and small wing area generate less lift forces than for a regular fixed-wing MAV. For this reason, the Golden Snitch adopts a high strength-to-mass ratio titanium alloy as the airframe material and parylene as the skin material of the flapping wing. Furthermore, a lightweight high-power battery was used in the design.

Determining an accurate size for the titanium-alloy airframe and its shaping using conventional machining methods without incurring residual stress is a challenging process. To mitigate this, a wet etching technique was used to tailor the airframe structures from the titanium-alloy plate, and tests showed no apparent residual stress. A parylene coating technique was used for laying the wing skin attached to the titanium frame.

Because flight tests show that flexible wing frames generate more lift than rigid wing frames, the MAV was remodeled using carbon-fiber wing frames with 30° ribs and a new gear transmission module. The body mass and wingspan were also reduced to approximately 8 g and 21.6 cm, respectively. Flight test results and aerodynamic performance analysis showed a 35% improvement in thrust. The removal of the structure reaming on pivoting joints and the penalty force from the unsteady flapping reduces friction losses, which is a net benefit of this design. Reduced friction in the mechanical transmission module boosted the wing beat frequency of the Golden Snitch MAV up to 20 Hz (much faster than our earlier designs).
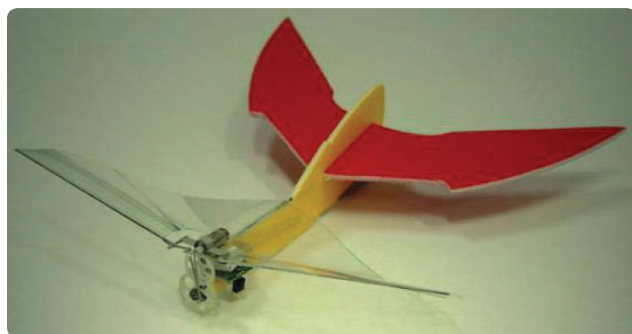

FIGURE 1 The flapping-wing micro aerial vehicle, the Golden Snitch, developed at Tamkang University. It is an 8-g weight and 20-cm wingspan aircraft, including the fuselage, flapping wings, tail wings, battery, motor, and gear system. The flapping wings are driven by a motor with a four-bar linkage system. By adjusting the lengths of the four bars, various stroke angles can be achieved. The stroke angle of the Golden Snitch is designed to be around 53° [3].

How Does a Stereovision System Work?

A stereovision system is designed to mimic the human eyes. Two types of geometry are usually designed to obtain stereo vision, the crossing method and the parallel method [22], as shown in Figure S1. This article selected the parallel method, which is easier to manipulate.

Consider an experimental setting as shown in Figure S2. Let the point P be the target to observe. Figure S3 shows the view of the left and the right camera, respectively. Define P_{max} as the largest pixel numbers counted from the central line and θ_{max} as the half field of view in the horizontal direction, as shown in Figure S4.

The x coordinate of the target is given by [23]

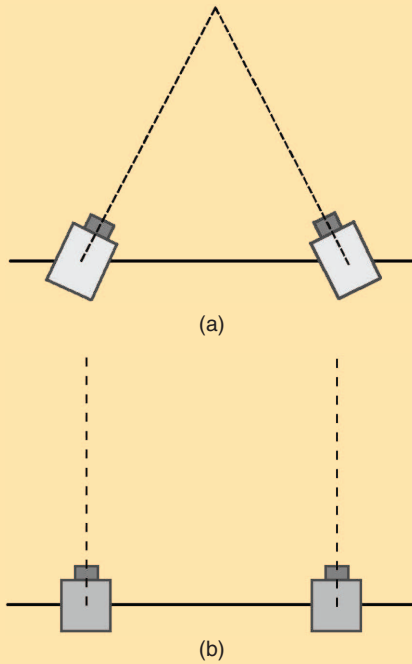$$x = C\left(\frac{1}{2} + \frac{1}{\rho - 1}\right), \tag{S1}$$

FIGURE S1 Geometries of the stereo camera. (a) Crossing method and (b) parallel method. The cross method resembles human eyes more than the parallel method [22]. This article selected the parallel method, which is easier to manipulate.
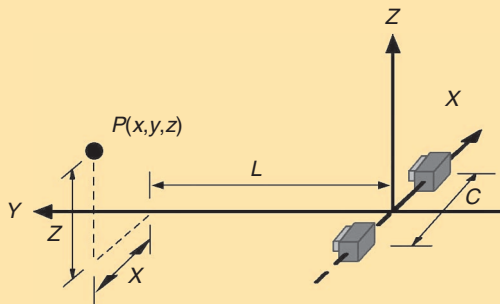
FIGURE S2 The definition of the camera coordinate system. The point P is the target to observe. The origin of the coordinate system is located at the center of two cameras. The x points to the left, y points toward the target, z is perpendicular to x and y, and C denotes the dispersion of the two cameras.
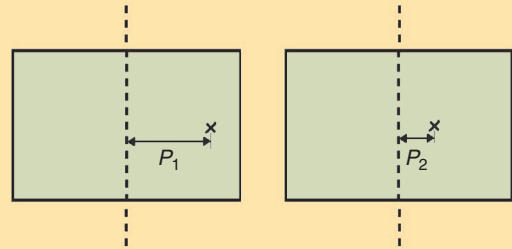
FIGURE S3 The vision of the two cameras. The cross mark denotes the target, and P_1 and P_2 denote the pixels deviated from the center of the vision, observed from the left and right cameras, respectively.
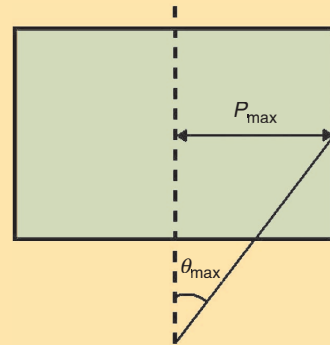
FIGURE S4 The vision of a camera and definition of parameters, with P_{max} denoting the largest pixel numbers deviated from the center of the picture in a horizontal direction and θ_{max} being the half field of view of the camera.
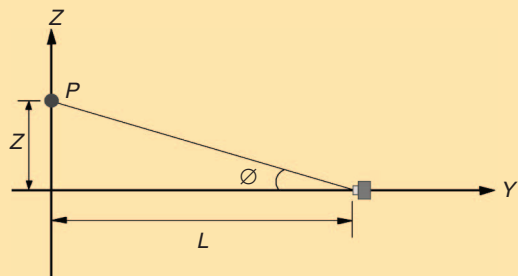
FIGURE S5 Definition of depth L and vertical vision angle ϕ. The geometry implies that $\tan\phi = z/L$.

where C is the dispersion of the two cameras, P_1 and P_2 are the pixels away from the center seen by the left and the right camera, respectively, and $\rho = P_1/P_2$. The depth $y = L$ is obtained by

$$L = \frac{C}{\gamma(\rho - 1)\tan\theta_{max}} \tag{S2}$$

where $\gamma := P_2/P_{max}$.

The height of the target is attainable through similar procedures. Define ϕ_{max} as the half field of view in the vertical direction. Similar derivations yield [23]

$$z = \mu \tan\phi_{max}, \tag{S3}$$

where $\mu = q/q_{max}$, and the definitions of q, q_{max}, and ϕ_{max} are depicted in Figures S5 and S6.
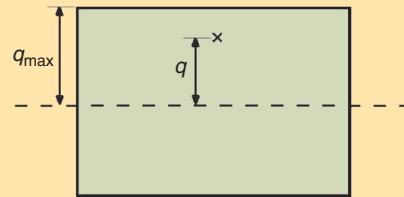

FIGURE S6 The vision of a camera and definition of parameters. The cross mark denotes where the target appeared in the picture, and q_{max} and q denote the maximal pixels and the pixels of the target counted from the center of the picture in the vertical direction, respectively.

The Wing Frame

The wing motion of a bird is a composite of flapping, twisting, folding, and gliding. To precisely reproduce such a rich motion set in a robotic bird would require highly sophisticated mechanisms. Instead of creating such a mechanism, a one-degree-of-freedom (1 DOF) flapping mechanism was designed to simplify the design and keep its weight down. This tradeoff means that the aerodynamic performance of this design will be less efficient than the wing motion of real birds. To compensate for this, the design uses a high flapping frequency. A wing frame that can sustain a higher flapping frequency requires high structural strength. Consequently, strength and weight of the materials for wing frames are crucial issues.

In our initial design, titanium-alloy wing frames were employed. Having tried different materials, carbon-fiber wing frames were found to generate more lift. Moreover, streamwise vibration of the carbon-fiber leading edge was characterized by a wingbeat frequency from 15.6 to 21.7 Hz for the wings with 30° ribs. This frequency is much smaller than the natural frequency of 85 Hz for the wing structure. Therefore this special vibration has no effect on the resonance of the wing frame. By combining this induced coherent streamwise vibration of the wing frame and the vertical reciprocating flapping motion shown in Figure 2, a stereo figure-of-eight flapping motion of the MAV shows up and can be seen even by the unaided human eye. This observation was validated by the use of LED illumination, as shown in Figure 3. This streamwise vibration of the wing frame is attributable to the Knoller-Betz effect [25] and interpreted as a coherent forward locomotion. The biggest thrust or the vibration amplitude occurs at the instants of stroke reversals, i.e., the highest and lowest points of the flapping motion. Our experiments show that a biomimetic figure-of-eight wing tip trajectory can be generated by a simple flapping mechanism in flexible MAVs.

Design of the Gear Transmission System

The gear transmission system for the MAV is composed of a gear-reduction set and a four-bar linkage, as shown in Figure 4. A 7-mm diameter DIDEL electric motor was installed to drive the transmission system. The gear set with a gear ratio of 26.6 provided sufficient torque for driving the flapping wings. The entire gear set and the motor were originally arranged on an aluminum base. In the Golden Snitch, however, the whole set was replaced by plastic pieces. Taking advantage of plastic injection molding, the pieces of the transmission system could be produced in large quantities of identical individual units. These identical gear sets not only lower the costs but also result in more reliable and repeatable experimental results.

DYNAMIC MODEL

The complete nonlinear dynamics of the Golden Snitch is discussed elsewhere [19]. This article only considers the equation of vertical motion, and focuses on the implementation of the altitude control law. Although realizing autonomous flight is the ultimate goal, the current stage only controls the flight altitude due to the particular mechanisms of the Golden Snitch. The chosen communication module and the design of the linkage system place constraints on the operation capability in flapping frequency and provide null ability for directional and attitude controls. Consequently, this article is primarily concerned with control, navigation, guidance, and implementation issues related to vertical motion.

From Newton's second law, the dynamics of vertical motion can be formulated as

$$\sum F_z = m\ddot{z}, \tag{1}$$

where F_z denotes the forces in the vertical direction, m is the mass of the flapping-wing MAV, z is the position in the vertical direction, and $\ddot{z}$ is the vertical acceleration. The external forces in (1) include the weight mg, the average lift
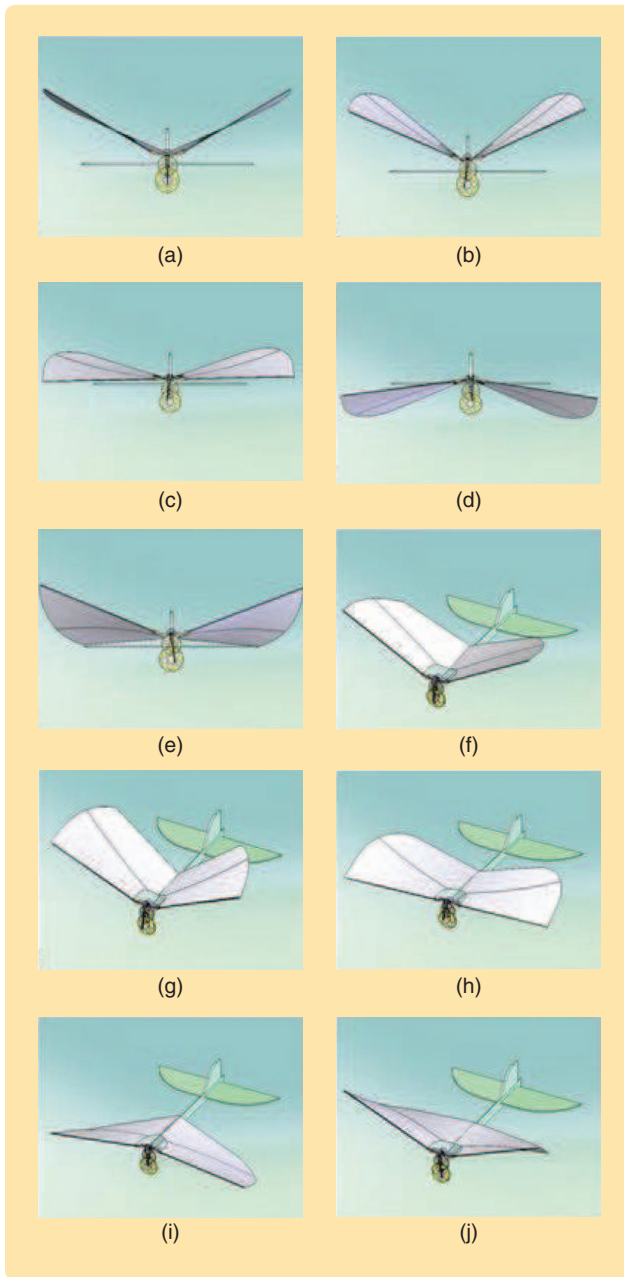
FIGURE 2 An illustration depiction of the continuous full-cycle flapping motion of the micro aerial vehicles with a rigid four-bar transmission module. (a) denotes the neutral position; (b) and (c) denote the downstroke; (d) and (e) denote the upstroke; the bird's-eye views from (f) to (j) correspond to the front side views from (a) to (e), respectively [3].
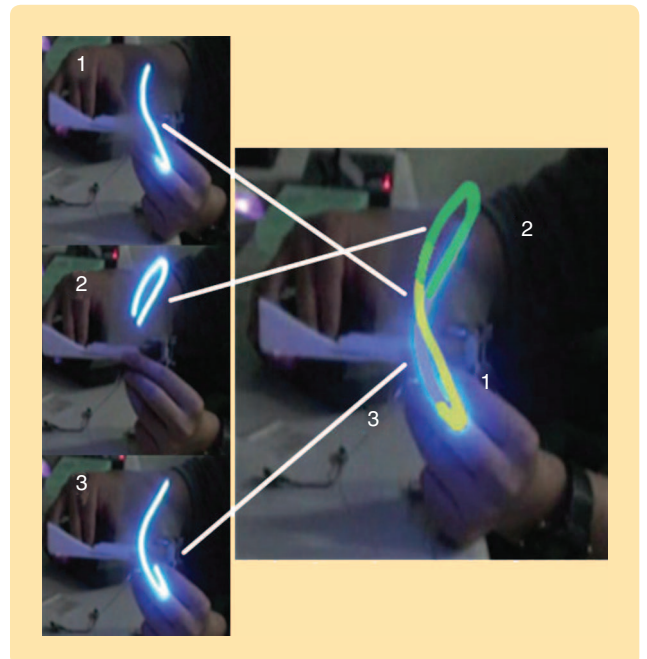

FIGURE 3 Wing tip trajectory traced out by LED illumination. Images 1–3 are instantaneous images of a figure-of-eight taken by a high-speed video camera. The right image combines the left three images [3].
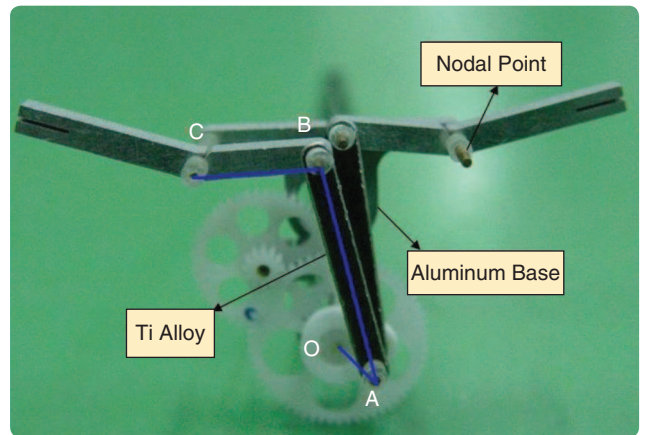

FIGURE 4 Gear transmission system. The aluminium base is used for wind tunnel tests, while the light plastic base is selected for an actual flight experiment [3].

force generated by the main wings F_w, and the lift force generated by the tails F_t. The upward direction is defined as positive, and the downward direction as negative. Note that F_w is the average lift force over one flapping period of around 0.08 s [19]. As a result, (1) describes the averaged motion longer than one flapping period, and the equations of motion are rewritten as

$$F_w + F_t - mg = m\ddot{z}. \tag{2}$$

The lift forces of the main wings and the tails are functions of the parameters [3], [19]

$$F_w = \frac{1}{2}\rho U^2 S_w C_{L_w}, \tag{3}$$

$$F_t = \frac{1}{2}\rho U^2 S_t C_{L_t}, \tag{4}$$

respectively, where ρ denotes the air density, U denotes the incoming wind speed, S denotes the area of the wings, and C_L denotes the lift coefficient. The subscripts w and t denote the main wings and the tails, respectively. To simplify future derivations, let $K_w = \rho S_w/2$ and $K_t = \rho S_t/2$.

Set Angle	10°	20°	30°	40°	50°
ζ	19.07	20.22	35.35	42.09	58.25
η	5.471	4.174	4.851	4.823	6.107
ξ	0.6914	1.181	1.404	2.051	2.346

TABLE 2 The values of the tail lift coefficient as a function of the angle of attack (AOA).

AOA	−20°	−10°	0°	10°
C_{L_t}	−1.242	−0.2808	0.3571	0.5963
AOA	20°	30°	40°	50°
C_{L_t}	0.6881	0.8148	0.9025	0.8868

The averaged lift coefficient generated by the main wings over one flapping period is given by

$$C_{L_w} = \zeta e^{-\eta J} + \xi, \tag{5}$$

where ζ, η, and ξ are parameters that are specified by the wings, and the *advanced ratio J* is defined as

$$J = \frac{U}{2bf\Phi}, \tag{6}$$

where Φ, f, and b are the stroke angle, flapping frequency, and semiwingspan, respectively.

The parameters ζ, η, and ξ in (5) are functions of the *set angle*, which is an angle set up in the wing tunnel test. Different from a fixed-wing aircraft, whose angle of attack remains constant provided the pitch angle of fuselage remains constant, the angle of attack of the flapping wings varies all the time. As a result, the conventional definition of angle of attack does not apply to flapping-wing MAVs. Instead, the set angle is commonly employed as a parameter when the aerodynamics of flapping-wing MAVs are investigated. When flight tests are discussed, the set angle equals the pitch angle of the fuselage plus the installed angle of the wings.

Although flapping aerodynamics has been theoretically investigated for many decades, they are not mature enough to predict the aerodynamic parameters in (5) analytically. So the model parameters in Table 1 were fit to experimental data collected by wind tunnel tests [3]. The experimental data of the tail lift coefficient as a function of the angle of attack provided in [19] are listed in Table 2.

HARDWARE

Unlike a regular unmanned aerial vehicle, in which control laws are easily implemented if the computational speed meets the real-time requirements, an MAV is highly constrained by size and weight restrictions. Consequently, when dealing with implementation of control laws and realization of autopilot of the Golden Snitch, these two factors must be taken into consideration.

Hardware Architecture

Figure 5 illustrates the traditional hardware architecture for the autonomous flight of unmanned aerial vehicles.
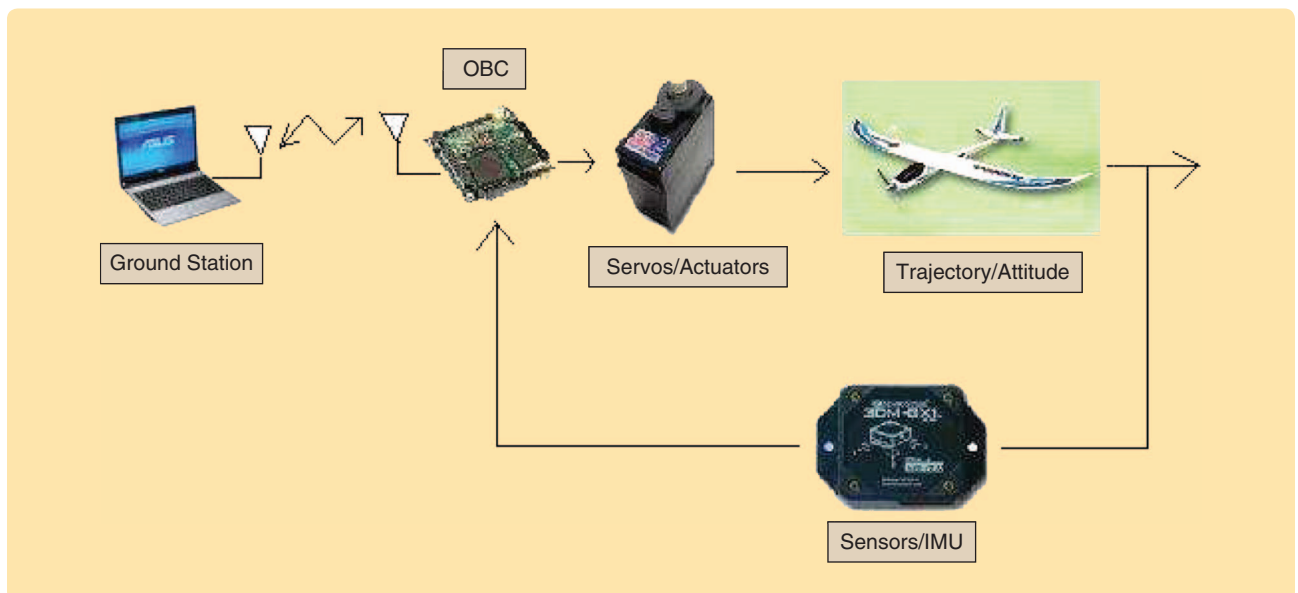

FIGURE 5 The traditional hardware architecture for the autonomous flight of unmanned aerial vehicles. Traditionally, an aircraft is equipped with an onboard computer for communicating with the ground station, receiving flight data from sensors or an inertial measurement unit (IMU), and calculating control commands based on a designed control law. In addition to an onboard computer, sensors and/or IMUs are present onboard to collect flight data; antennas and encoder/decoder are also essential for communication. The trajectory of the vehicle is preassigned or guided by the ground station through the communication module.

Traditionally an aircraft is equipped with an onboard computer responsible for communicating with the ground station, receiving flight data from sensors or an inertia measurement unit (IMU), and calculating control commands based on designed control law. In addition to an onboard computer, sensors or an IMU are essential for collecting flight data; and antennas and an encoder/decoder are also essential for communication. The trajectory of the vehicle is usually preassigned or guided by the ground station through the communication module.

The specifications of the Golden Snitch, however, are designed to keep the total weight of the vehicle under 10 g. If a traditional architecture is applied, the lightest radio frequency (RF) communication module, including an encoder and decoder, is approximately 3 g and the MEMS gyroscope is about 30 g. Installing these sensors on board would be too cumbersome, let alone installing a computer or microchips with supporting circuits.

A modified architecture is depicted in Figure 6. In this loop the traditional RF communication module is replaced by a 1-g IR module. Sensors to obtain the flight altitude are replaced by a set of external stereovision systems. Moreover, instead of using an onboard computer, control commands are computed on the ground station and then transmitted to the aerial vehicle. As a result, no control or sensing units are installed onboard. Although this structure limits the flight capability and applicability of a flapping-wing MAV to some extent, it is the most effective method to realize automatic control of flight altitude at gross vehicle weights fewer than 10 g. As technology advances, it is likely that an appropriate combination of sensors for complete onboard operation will become available.

Communication Module

A commercial IR communication module was employed because a regular RF communication module is too heavy to install on the Golden Snitch. The signal from the IR module is digital and composed of thrust and directional information. Currently, no mechanism has been designed to control the direction of the Golden Snitch, and only the control of thrust is discussed in this article. The control of the thrust was accomplished by a pattern of 4-bit code,
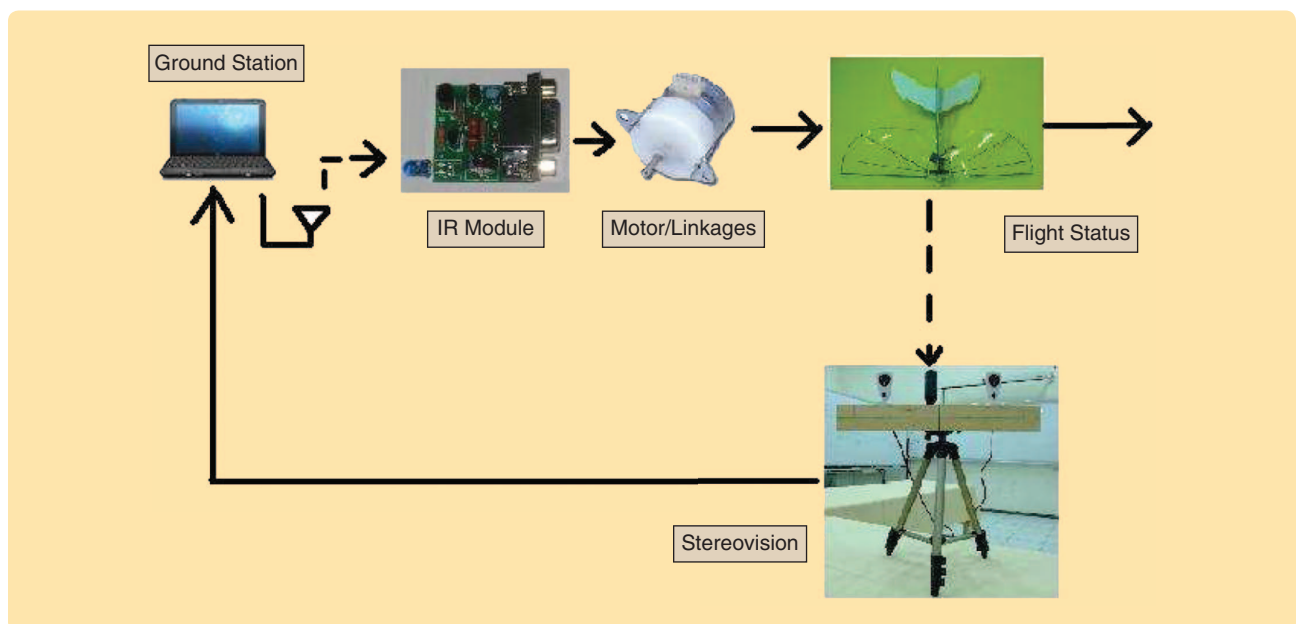

FIGURE 6 A modified control architecture for a micro aerial vehicle fewer than 10 g. In this loop, the traditional radio frequency communication module is replaced by a 1-g infrared module, and sensors to determine the flight altitude are replaced by a stereovision system. Moreover, instead of using an onboard computer, control commands are computed in the ground station and then transmitted to the aerial vehicle. As a result, no control or sensing units are on board.

TABLE 3 The thrust level and the average flapping rate.

Thrust Level (#)	Flapping Rate (Hz)	Thrust Level (#)	Flapping Rate (Hz)	Thrust Level (#)	Flapping Rate (Hz)
0	0	5	11.9	10	12.35
1	10	6	12.35	11	12.5
2	11.1	7	12.35	12	12.66
3	11.76	8	12.19	13	12.8
4	11.76	9	12.35	14	12.8

implying that at most 16 levels of thrust can be provided, including zero input. In actuality, only 14 signals, zero input excluded, was used in thrust control. The 14 signals control the 14 spin rates of the driving motor, which then convert to 14 flapping frequencies through the four-bar linkage. The relation between thrust levels and the corresponding flapping frequencies are given in Table 3.

The use of this IR module raises a potential control problem. Due to the protocol of the IR module, only 14 nonzero and discrete flapping frequencies are available, implying that only limited amounts of control signals are allowed to manipulate the MAV. As a result, traditional control laws may need to be modified before they are applied.
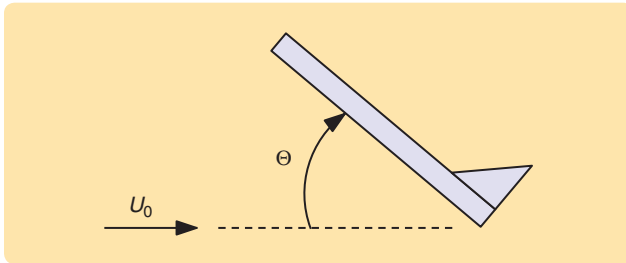

FIGURE 7 Definition of parameters at cruise flight. The aircraft experiences an incoming stream of speed U_0, when flying forward with a nominal speed U_0 and fuselage pitch angle Θ.
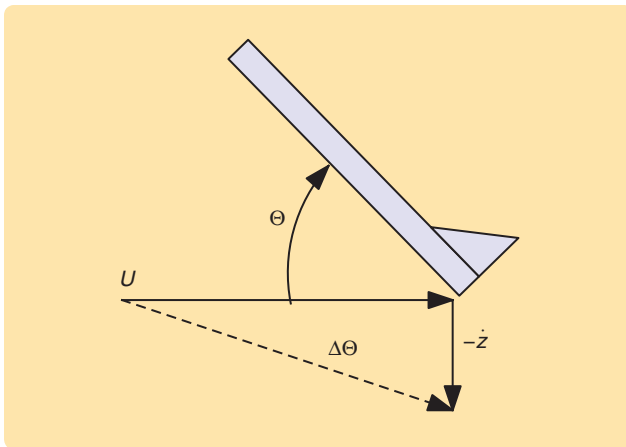

FIGURE 8 Definition of parameters for vertical motion. When a vehicle moves upward with speed $\dot{z}$, the vertical motion induces a decrease in the angle of attack by $\Delta\Theta$, where $\tan\Delta\Theta = \dot{z}/U$.

CONTROL LAW DESIGN

As stated previously, this article does not present a new or more sophisticated control law but mainly focuses on hardware implementation and system integration. Accordingly, a modified P-control is investigated and shown to be adequate in this case.

Linearized Dynamics

The nonlinear dynamics describing the altitude of the vehicle is given in (2). For initial analysis purposes, the Golden Snitch was assumed to be initially cruising at a height of $z = z_0$ with a speed of $U = U_0$, in which the corresponding flapping frequency was assumed to be $f = f_0$. The autopilot was in charge of maintaining the flapping-wing MAV in the cruise condition. For the MAV encountering a small perturbation, the excursion of the vehicle from the nominal condition was characterized by linearizing the nonlinear equations of motion about this nominal condition.

Assume that the vehicle is initially operating under cruise conditions, namely, $z = z_0$, $\dot{z} = 0$, $U = U_0$, and $f = f_0$. Let $\Theta(t)$ be the pitch angle of the fuselage in Figure 7 and assume that $\Theta = \Theta_0$ at cruise. The set angle for the main wings is approximately $\alpha_w = \Theta_0 + c_w$, while the angle of attack (AOA) of the tails is $\alpha_t = \Theta_0 + c_t$, where c_w and c_t are constants that depend on the installation angle of the wings.

On the other hand, when the vehicle moves upward at a vertical speed $\dot{z}$, the AOA decreases by

$$\Delta\Theta = \tan^{-1}\frac{\dot{z}}{U}, \tag{7}$$

as depicted in Figure 8. Let

$$F_w = F_{w,0} + \delta F_w, \tag{8}$$

$$F_t = F_{t,0} + \delta F_t, \tag{9}$$

$$z = z_0 + \delta z, \tag{10}$$

where $F_{w,0}$ and $F_{t,0}$ denote the required lift forces generated by the main wings and the tail wings, respectively, δF_w and δF_t denote the perturbations in lift forces generated by the main wings and the tail wings, respectively, and δz denotes the offset of the flapping-wing MAV from the nominal altitude. The linearization of (2) is then given by

$$\delta F_w + \delta F_t = m\delta\ddot{z}. \tag{11}$$

Equations (3) and (5) suggest that the force generated by the main wings is a function of U, ζ, η, ξ, and J. In addition, J itself is a function of the flapping frequency f. Therefore, the dependencies can be written as

$$F_w = F_w(U, \zeta, \eta, \xi, f)$$

so that the perturbation δF_w can be formulated as:

$$\delta F_w = \frac{\partial F_w}{\partial U}\delta U + \frac{\partial F_w}{\partial \zeta}\delta\zeta + \frac{\partial F_w}{\partial \eta}\delta\eta + \frac{\partial F_w}{\partial \xi}\delta\xi + \frac{\partial F_w}{\partial J}\delta J. \tag{12}$$

According to the wind tunnel tests, the parameters (ζ, η, ξ) are functions of the set angle. Assume that the vehicle suffers from deviations in its vertical position and speed, denoted by δz and $\delta\dot{z}$, respectively. Figure 8 indicates that these deviations induce variations in the parameters by changing the direction of the injecting flow, which is equivalent to changing the set angle.

Accordingly, the variations in those parameters are attainable from the derivations

$$\delta U = \frac{\partial U}{\partial\dot{z}}\delta\dot{z}$$
$$= \frac{\partial}{\partial\dot{z}}\sqrt{U_0^2 + \dot{z}^2}\Big|_{U=U_0, \dot{z}=0}\delta\dot{z}$$
$$= 0, \tag{13}$$

$$\delta\zeta = \frac{\partial\zeta}{\partial\Theta}\delta\Theta = \frac{\partial\zeta}{\partial\Theta}\frac{\partial\Theta}{\partial\dot{z}}\delta\dot{z}, \tag{14}$$

$$\delta\eta = \frac{\partial\eta}{\partial\Theta}\delta\Theta = \frac{\partial\eta}{\partial\Theta}\frac{\partial\Theta}{\partial\dot{z}}\delta\dot{z}, \tag{15}$$

$$\delta\xi = \frac{\partial\xi}{\partial\Theta}\delta\Theta = \frac{\partial\xi}{\partial\Theta}\frac{\partial\Theta}{\partial\dot{z}}\delta\dot{z}. \tag{16}$$

Equations (13)–(16) suggest that the variation of parameters is a function of the variation of the set angle induced by the speed perturbation. Hence, it is useful to obtain $\partial\Theta/\partial\dot{z}$ analytically. According to Figure 8,

$$\frac{\partial\Theta}{\partial\dot{z}} = -\frac{d}{d\dot{z}}\left(\tan^{-1}\frac{\dot{z}}{U}\right)\Big|_{U=U_0, \dot{z}=0} = -\frac{1}{U_0}. \tag{17}$$

On the other hand, the variation of J due to a flapping frequency perturbation δf is given by

$$\delta J = \frac{\partial J}{\partial f}\delta f = \frac{-U_0}{2b\Phi f_0^2}\delta f. \tag{18}$$

As a result, the perturbation of F_w is expanded as

$$\delta F_w = -\frac{1}{U_0}\left(\frac{\partial F_w}{\partial\zeta}\frac{\partial\zeta}{\partial\Theta} + \frac{\partial F_w}{\partial\eta}\frac{\partial\eta}{\partial\Theta} + \frac{\partial F_w}{\partial\xi}\frac{\partial\xi}{\partial\Theta}\right)\delta\dot{z}$$
$$+ \frac{-U_0}{2b\Phi f_0^2}\frac{\partial F_w}{\partial J}\delta f$$

$$= -K_w U_0\left(e^{-\eta J}\frac{\partial\zeta}{\partial\Theta} - J\zeta e^{-\eta J}\frac{\partial\eta}{\partial\Theta} + \frac{\partial\xi}{\partial\Theta}\right)\delta\dot{z}$$
$$+ \frac{-U_0}{2b\Phi f_0^2}\frac{\partial F_w}{\partial J}\delta f. \tag{19}$$

Similarly, the perturbation of F_t is attainable by

$$\delta F_t = \frac{\partial F_t}{\partial\Theta}\delta\Theta = K_t U_0^2\frac{\partial C_{L_t}}{\partial\Theta}\frac{\partial\Theta}{\partial\dot{z}}\delta\dot{z} = -K_t U_0\frac{\partial C_{L_t}}{\partial\Theta}\delta\dot{z}. \tag{20}$$

Denote the partial derivative of a parameter X with respect to Θ as $X_{,\Theta}$ in the following derivations. The linearized equations of motion are then formulated as

$$m\delta\ddot{z} + B\delta\dot{z} = R\delta f, \tag{21}$$

where

$$B = K_w U_0(e^{-\eta J}\zeta_{,\Theta} - J\zeta e^{-\eta J}\eta_{,\Theta} + \xi_{,\Theta}) + K_t U_0 C_{L_t,\Theta}, \tag{22}$$

$$R = K_w U_0^2\zeta\eta e^{-\eta J}\frac{U_0}{2b\Phi f_0^2}. \tag{23}$$

Control Law Design

Equation (21) provides the linearized equations of vertical motion of the Golden Snitch. The open-loop transfer function of this system is given by

$$\frac{\delta z(s)}{\delta f(s)} = \frac{R}{ms^2 + Bs}. \tag{24}$$

Since the open-loop system has one pole at the origin and the other pole in the left-hand plane, a simple P-control with unity feedback is enough to stabilize the system, regardless of the value of the feedback gain K. If the MAV is to be maintained at the nominal height, we require the reference command to be zero in the linearized dynamics. The reference command is the height for the system to track over time, with the nominal height $z(t) = z_0$. As a result, the reference command in the linearized system, which only considers the offset dynamics, is given by $\delta z_r = z - z_0 = 0$ from (10). The control of the linearized system is then given by

$$\delta f(s) = -K\delta z(s) + \delta z_r = -K\delta z(s). \tag{25}$$

Or, $\delta f(t) = -K\delta z(t)$ in the time domain.

When considering the Golden Snitch, however, the discontinuity of control caused by the limited communication capability also has to be considered. As stated in the preceding sections, 14 nonzero flapping frequencies, denoted by $\{f_{0_1}, f_{0_2}, \dots f_{0_{14}}\}$, can be used for cruise flight. It is important to recall that $\delta f(s)$ in (25) actually denotes the *frequency variation*, meaning $\delta f = f - f_0$. Assume that the required flapping frequency for a specific cruise condition is f_{0_i}. The available frequency variations under this circumstance are the sequence $\delta f = \{\Delta f_k\}$, where $\Delta f_k = f_{0_k} - f_{0_i}$, $k = 1, \dots, 14$.

TABLE 4 Physical parameters for the Golden Snitch.

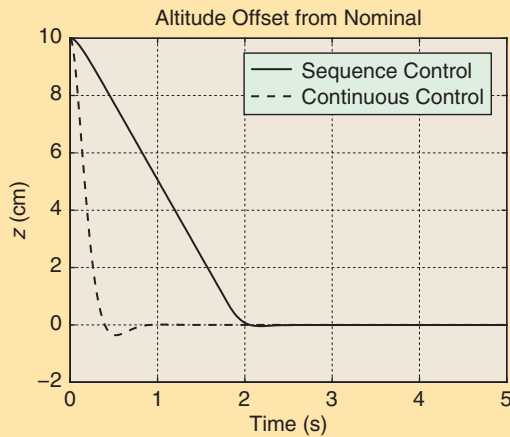| Item	Value	Item	Value
m	8	Θ	0.3491
b	0.2	η	4.174
f_o	12.66	$\eta_{,\Theta}$	1.1007
ζ	20.22	S_t	0.006
ζ_Θ	57.4276	U_0	3.5
$C_{L,\Theta}$	2.1985	Φ	0.925
S_w	0.014	ξ	1.181
ρ	1230	$\xi_{,\Theta}$	2.3945

FIGURE 9 Numerical simulation of altitude variation under altitude perturbation. After an initial perturbation of 10 cm in height, the control law brings the vehicle back to the nominal height successfully. However, due to the discontinuity of the control command in actual practical implementation, the control history is less efficient.
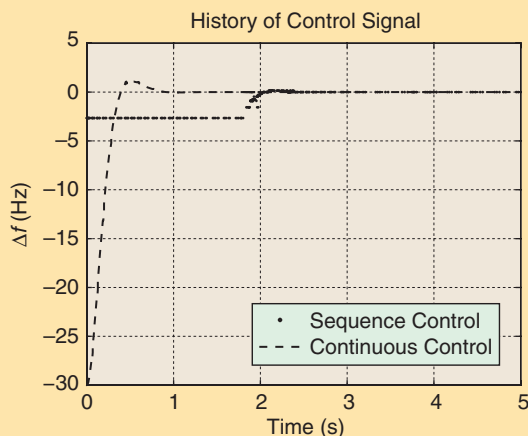

FIGURE 10 Numerical simulation of the control history.

Since only limited choices of frequency variations are available for use as the control command, the position feedback $\delta f = -K\delta z$ in (25) computed with a predesigned feedback gain K is rounded to the nearest element in the control sequence Δf_k. Numerical simulations shows the validity of this method for this particular system and on the convergence of the system to the desired state.

NUMERICAL SIMULATIONS

The physical parameters of the Golden Snitch are in Table 4. The unit for length is m; for mass, g; for frequency, Hz; for angle, rad; and for the derivatives, 1/rad. For the parameters shown in Table 4, the variables defined in (23) and (22) are computed as $R = 2.0541$ and $B = 102.0409$. From root-locus analysis, the damping ratio is about 0.7 when $K = 300$.

Figures 9 and 10 provide numerical simulations of the modified proportional control law, compared to a regular P-control. The vehicle is assumed to initially suffer from a vertical position offset by +10 cm. Later the control law begins to work and returns the vehicle back to the nominal height, as shown in Figure 9. Figure 10 demonstrates the control history. The solid line denotes the history by a regular continuous P-control, whereas the dashed line denotes the history under the developed control law.

Due to the discontinuity of the control, the developed algorithm is less efficient than the regular P-control, and the response of the closed-loop system is slower. However, the altitude remains stable under this algorithm.

EXPERIMENTS AND DISCUSSION

Flight Tests Inside the Laboratory

Two types of flight tests were arranged. The first type of flight test was accomplished inside the laboratory and designed to measure quantitative properties, whereas the second type was performed within an indoor open space to verify the qualitative performance of the entire loop. Examples of these experiments are shown in Figures 11 and 12, and a video showing the experiments is available [24].

Due to space constraints in the laboratory, the MAV was attached to the ceiling with a string of negligible mass, which forces the MAV to fly within a certain range. The length of the string is such that it is not enough to influence its vertical motion. Although the string becomes tight to provide centripetal force when the MAV is flying, any deviation from the nominal altitude still results in corrective control action. By flying faster or slower, the robotic bird can adjust itself to the designated nominal altitude. The system loop is constructed as seen in Figure 6, in which the altitude of the MAV is measured by the computer stereovision system. Several blue stripes were placed on the wall, as shown in Figure 11, denoting 1.8, 1.6, 1.4, and 1.2 m, respectively, from top to bottom, to provide visual references for human operators.

FIGURE 11 Flight tests in the laboratory. The micro aerial vehicle (MAV) is tethered to the ceiling with a string of negligible mass to force it to fly within a certain range. The blue stripes on the wall, denoting 1.8 m, 1.6 m, 1.4 m, and 1.2 m, respectively, from top to bottom, are set to provide visual references for human operators. The MAV is highlighted by a red circle. The MAV flies around the preassigned cruise altitude $h = 1.5$ m. These pictures are snapshots from a video [24]. The MAV is highlighted and the clock was post-edited with a photo editor.

The measured results are shown in Figures 13–15. In Figures 13 and 14 the nominal altitudes were set at 1.5 and 1.2 m, respectively. Although the MAV is noisy at the measured height, it is apparent that the Golden Snitch hovers around the vicinity of the assigned altitudes. Due to the limited control sequences, the largest control that can be applied is –2.5 Hz, corresponding to an excursion of $250/K$ cm,

where K is the designed feedback gain. That is, any excursion measurement larger than $250/K$ cm is going to be filtered and only triggers the largest control signal. As a result, the noisy observation did not cause large variation in the flight tests.

In Figure 15, the flapping-wing MAV originally cruised at an altitude of 1.2 m. The new nominal altitude was set to
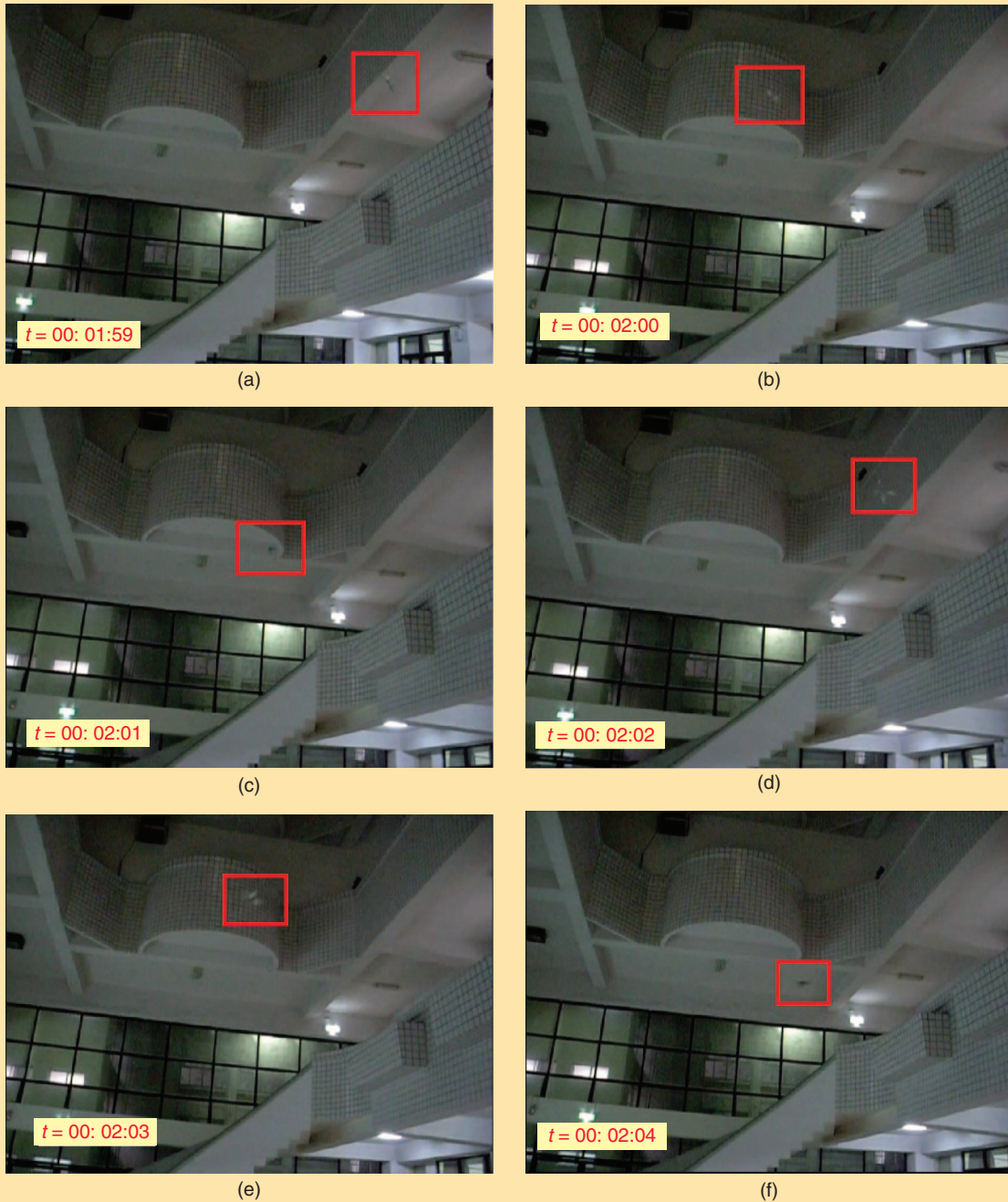
FIGURE 12 Flight tests in an indoor open space. The micro aerial vehicle (MAV) is highlighted by a red square. Because no additional methods are available to cross-check the measurements by the stereovision in the open space, the structure of the system loop was verified only qualitatively. It is shown from pictures that the Golden Snitch is maintained at a range of heights under the control of the developed structure. These pictures are snapshots from a video [24]. The MAV is highlighted and the clock was post-edited with a photo editor.

be 1.5 m, and the corresponding nominal thrust level was also provided. The figure shows that the flapping-wing MAV starts to be brought to the new nominal altitude at the 35th data point, corresponding to $t = 10.5$ s, although measurement error exists [23]. When the new nominal height was set, the MAV, cruising at the original nominal height, is viewed as having initial excursion of −30 cm from the nominal. Hence, the proposed control law is expected to work and compensate for the excursion. Figure 15 shows that the control does function to compensate the excursion and try to maintain the MAV at the designated height.
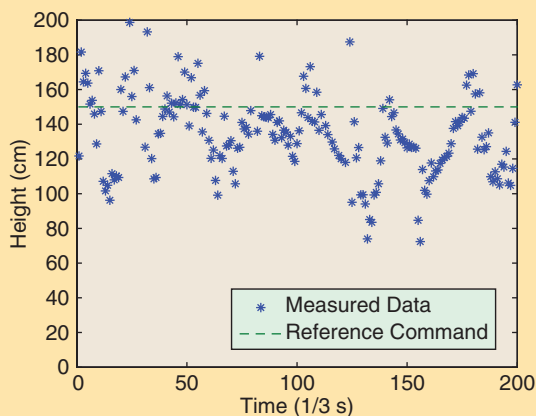
FIGURE 13 Position data acquired by the stereovision system. The nominal altitude was 1.5 m. Although the data are noisy, Figure 11 suggests that the noise comes from the stereovision system. Moreover, Figure 11 shows that the control keeps the robotic bird flying around the nominal height even under noisy feedback. These are the data sets from the flight tests inside the laboratory.
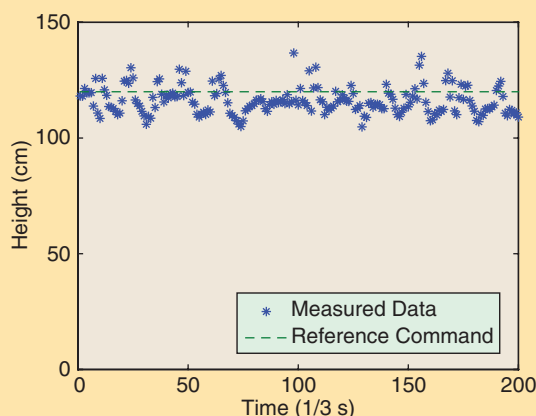
FIGURE 14 Position data acquired by the stereovision system. The nominal altitude was 1.2 m. Although the data are noisy, Figure 11 suggests that the noise comes from the stereovision system. Moreover, Figure 11 shows that the control keeps the robotic bird flying around the nominal height even under noisy feedback. These are the data sets from the flight tests inside the laboratory.
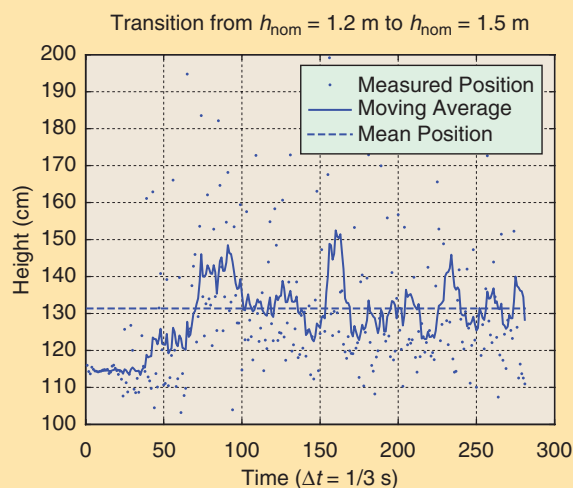

FIGURE 15 Altitude transition from a height of 1.2 m to 1.5 m. Plot (a) shows the altitude history, and plot (b) shows the control history. In this flight test, the flapping-wing MAV originally cruised at an altitude of 1.2 m. The new nominal altitude was set to be 1.5 m, and the corresponding nominal thrust level was also provided. The plots show that the flapping-wing MAV starts to be brought to the new nominal altitude at the 35th data point, corresponding to $t = 10.5$ s, though measurement error exists.
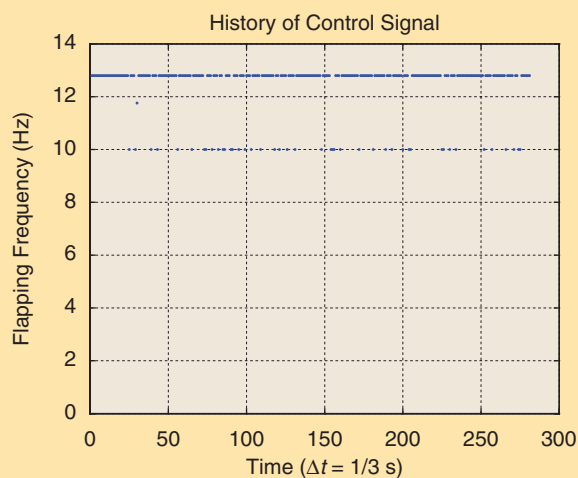
Figure 11 also provides additional evidence that the altitude of the MAV lingers around the designed 1.5 m. We conclude that the variation of the observed data comes from the measurement of noise by the stereovision system, and this system is expected to improve in the future. However, these flight tests do quantitatively verify the function of the control law.

Flight Tests in an Indoor Open Space

The flight tests in an indoor open space are shown in Figure 12. Since no additional methods are available to cross-check the measurements by the stereovision in open space, these tests only qualitatively verify the structure of the system loop. Although we currently do not know the vehicle's flight capabilities regarding altitude, the Golden Snitch appears to cruise at a certain altitude under the control of the proposed scheme.

CONCLUSION

This article described a control law for stabilizing the vertical motion of a flapping-wing MAV and developed a system architecture that is potentially beneficial in realizing the autonomous flight of flapping-wing MAVs fewer than 10 g. The article began with a brief introduction to the Golden

Snitch, including its development history and the development of the overall system. The vertical dynamics were given for altitude control. The use of wind tunnel tests to obtain aerodynamical parameters was described. Due to the limited payload-carrying capability, the control architecture was modified so that automatic control of flight altitude of a flapping-wing MAV fewer than 10 g is possible using current technology. Taking the hardware constraint into account, it was shown that the modified P-control can stabilize the vertical motion and track altitude commands. Numerical simulations and flight tests were presented that demonstrate the function of the developed control law and the system architecture. We believe this flapping-wing MAV to be the first under 10 g able to automatically maintain its flight altitude.

ACKNOWLEDGMENT

AUTHOR INFORMATION

Fu-Yuen Hsiao (fyhsiao@mail.tku.edu.tw) received the B.S. degree from the National Cheng-Kung University in Taiwan in 1997 and the master's and Ph.D. degrees in 2002 and 2004 from the Department of Aerospace Engineering at the University of Michigan. He is currently an assistant professor in the Department of Aerospace Engineering at Tamkang University, Taiwan. His research interests include astrodynamics, flight dynamics and control of unmanned aerial vehicles and flapping-wing aerial vehicles, and applications of image processing. He can be contacted at the Department of Aerospace Engineering, Tamkang University, 151 Ying-zhuan Rd., Tamsui, New Taipei, 25137, Taiwan.

Lung-Jieh Yang received the B.S. degree from the National Cheng-Kung University, the master's degree from Tamkang University in 1991, and the Ph.D. degree from National Taiwan University. He is currently a full professor in the Department of Mechanical and Electro-Mechanical Engineering at Tamkang University, Taiwan. His research interests include microelectromechanical systems, micro fluids, and flapping-wing aerial vehicles.

Sen-Huang Lin received the B.S. and master's degrees from the Department of Aerospace Engineering at Tamkang University, Taiwan, in 2007 and 2009, respectively. His research interests include flight dynamics and control of flapping-wing aerial vehicles.

Cheng-Lin Chen received the B.S. and master's degrees from the Department of Aerospace Engineering at Tamkang University, Taiwan, in 2006 and 2008, respectively. His research interests include applications of image processing.

Jeng-Fu Shen received the B.S. and master's degrees from the Department of Aerospace Engineering at Tamkang University, Taiwan, in 2003 and 2005, respectively. His research interests include navigation and guidance laws. He is currently a senior engineer in the Primax Electronics Ltd.

REFERENCES

[1] U. M. Norberg, *Vertebrate Flight: Mechanics, Physiology, Morphology, Ecology and Evolution*. New York: Springer-Verlag, 1990.
[2] U. Pesavento and Z. J. Wang, "Flapping wing flight can save aerodynamic power compared to steady flight," *Phys. Rev. Lett.*, vol. 103, no. 11, pp. 118012-1–118012-4, 2009.
[3] C. K. Hsu. (2008). The preliminary design, fabrication, and testing of flapping micro aerial vehicles, Ph.D. dissertation, Tamkang Univ., Taipei [Online]. Available: tkuir.lib.tku.edu.tw:8080/dspace/handle/987654321/35320
[4] J. Lighthill, *Mathematical Biofluiddynamics*. Philadelphia, PA: SIAM, 1975.
[5] B. Parslew, "Low order modelling of flapping wing aerodynamics for real-time model based animation of flapping flight," M.Sc. thesis, School of Mathematics, Univ. Manchester, U.K., 2005.
[6] M. S. Couceiro, N. M. F. Ferreira, and J. A. Tenreiro Machado. (2010). Modeling and control of a dragonfly-like robot. *J. Control Sci. Eng.*, vol. 2010. [Online]. Available: http://www.hindawi.com/journals/jcse/2010/643045/
[7] T. Weis-Fogh and M. Jensen, "Biology and physics of locust flight—Part I: Basic principles in insect flight. A critical review," *Philos. Trans. R. Soc. Lond. B*, vol. 239, no. 667, pp. 415–458, 1956.
[8] C. P. Ellington, "The aerodynamics of hovering insect flight," *Philos. Trans. R. Soc. Lond. B*, vol. 305, pp. 1–181, 1984.
[9] A. P. Willmott, C. P. Ellington, and A. L. R. Thomas, "Flow visualization and unsteady aerodynamics in the flight of the hawkmoth, *Manduca sexta*," *Philos. Trans. R. Soc. Lond. B*, vol. 352, pp. 303–316, 1997.
[10] G. C. H. E. de Croon, K. M. E. de Clercq, R. Ruijsink, B. Remes, and C. de Wagter, "Design, aerodynamics, and vision-based control of the DelFly," *Int. J. Micro Air Vehicles*, vol. 1, no. 2, pp. 71–97, 2009.
[11] Z. J. Wang, J. M. Birch, and M. H. Dickinson, "Unsteady forces and flows in low Reynolds number hovering flight: Two dimensional computations vs. robotic wing experiments," *J. Exp. Biol.*, vol. 207, pp. 449–460, 2004.
[12] X. Deng, L. Schenato, W. C. Wu, and S. S. Sastry, "Flapping flight for biomimetic robotic insects—Part I: System modeling," *IEEE Trans. Robot.*, vol. 22, no. 4, pp. 776–788, Aug. 2006.
[13] J. Yan, R. J. Wood, S. S. Avadhanula, and R. S. M. Fearing, "Towards flapping wing control for a micromechanical flying insect," in *Proc. IEEE Int. Conf. Robotics and Automation*, 2001, pp. 3901–3908.
[14] L. Schenato, D. Campolo, and S. Sastry, "Controllability issues in flapping flight for biomimetic MAVs," in *Proc. 42nd IEEE Conf. Decision and Control*, 2003, pp. 6441–6447.
[15] D. Campolo, L. Schenato, E. Guglielmelli, and S. S. Sastry. (2005). A Lyapunov-based approach for the control of biomimetic robotic systems with periodic forcing inputs—Part 1. in *Proc. 16th IFAC World Congress*, Praha, Czech Republic, vol. 16. [Online]. Available: http://www.ifac-papersonline.net/Detailed/28657.html
[16] D. K. Kim and J. H. Han, "Smart flapping wing using macro-fiber composite actuators," in *Proc. Smart Structures and Materials*, 2006, vol. 6173, pp. 1–9.
[17] H. Rifai, N. Marchand, and G. Poulin, "Bounded attitude control of a biomimetic flapping robot," in *Proc. 2007 IEEE Int. Conf. Robotics and Biomimetics*, Sanya, China, pp. 1–6.
[18] Z. A. Khan and S. K. Agrawal, "Control of longitudinal flight dynamics of a flapping-wing micro air vehicle using time-averaged model and differential flatness based controller," in *Proc. 2007 American Control Conf.*, pp. 5284–5289.
[19] T. M. Yang and F. Y. Hsiao, "Dynamics of flapping micro-aerial vehicles," in *Proc. 2009 American Control Conf.*, St. Louis, MO, pp. 4190–4195.
[20] M. S. Couceiro, N. M. F. Ferreira, and J. A. Tenreiro Machado, "Application of fractional algorithms in the control of a robotic bird," *J. Commun. Nonlinear Sci. Numerical Simulation*, vol. 15, no. 4, pp. 895–910, Apr. 2010.
[21] F. G. Bermudez and R. Fearing, "Optical flow on a flapping wing robot," in *Proc. 2009 IEEE/RSJ Int. Conf. Intelligent Robots and Systems*, pp. 5027–5032.
[22] J.-S. Lee, C. W. Seo, and E. S. Kim, "Implementation of opto-digital stereo object tracking system" *Opt. Commun.*, vol. 200, pp. 73–85, 2001.
[23] C. L. Chen and F. Y. Hsiao, "Attitude acquisition using stereo-vision methodology," in *Proc. Visualization, Imaging, and Image Processing (VIIP 2009)*, Cambridge, U.K., Paper 652-108.
[24] Flight test of Golden Snitch [Online]. Available: http://www.youtube.com/watch?v=bexOl4YNnd0
[25] K. D. Jones, C. M. Dohring, and M. F. Platzer, "Experimental and computational investigation of the Knoller-Betz effect," *AIAA J.*, vol. 36, pp. 1240–1246, 1998.